Doppler Sonar and Surface Waves: Range and Resolution

JEROME A. SMITH

Scripps Institution of Oceanography, La Jolla, California

(Manuscript received 21 July 1988, in final form 27 January 1989)

ABSTRACT

The performance limitations of an acoustic Doppler sonar system are explored and compared with anticipated requirements for the measurement of surface wave directional/frequency spectra. To obtain measurements to a range D requires a delay Δt between pings long enough for sound to propagate out to D and back: $\Delta t(c/2) \geq D$. This defines a Nyquist frequency, ω_N (radians s^{-1}). Linear dispersion relates this to a "matched wavenumber," $k_N = \omega_N^2/g$. Waves travelling obliquely and harmonics of longer waves appearing at ω_N all have smaller wavenumbers, $k \leq k_N$; thus, k_N defines a maximum wavenumber requirement, or (equivalently) a matched range resolution, ΔR. From idealized surface wave spectra, the velocity resolution ΔV required to measure spectra out to (ω_N, k_N) can be estimated. For a given sonar "tone," the error-product $E = \Delta R \Delta V$ is a constant, so velocity resolution and range resolution must be traded off. The error product decreases with increasing acoustic frequency f_0 and number of tones. Higher frequency sound is also attenuated more rapidly, limiting the maximum range attainable. A practical approach is to define a desired range D, find the highest frequency which can be detected to that range, and then determine the number of tones required to achieve the target velocity and range resolutions. If too many tones are needed, a slight retreat in range resolution yields a relaxation in the velocity requirement as well (because of the steep spectral slope of surface wave spectra). Electronic design and performance is neglected here, on the presumption that the physical limits discussed will eventually be the important ones.

1. Introduction

In a previous paper (Pinkel and Smith 1987), it was shown that Doppler sonar systems are well suited to the measurement of surface waves and swell in the open ocean. Using two sonar beams oriented in different directions along the underside of the sea surface, we were able to estimate the three-dimensional (wavenumber and frequency) spectrum of surface wave energy, over space and time scales appropriate to swell and near-peak frequency wind-waves. The sonars described in the previous paper were designed to measure lower-frequency mixed layer motion associated with internal waves, Langmuir circulation, etc. For this, they performed satisfactorily (Smith, Pinkel, and Weller 1987). They were not designed to measure surface waves. The fact that they did well in this too indicates that (i) the technique is well suited to surface waves, as noted, and (ii) it should be possible to do better.

Here, the issues involved in designing an acoustic Doppler system for surface wave measurement are addressed. For this purpose, it is useful to have in mind (i) an idealized surface wave spectrum, with which to estimate the velocity signal strength as a function of frequency and direction; and (ii) an idealized sonar beam configuration simple enough to analyze yet general enough to be useful.

Existing model spectra of surface waves are adequate to estimate the velocity signal levels, although there may be an order of magnitude of variation in the spectral levels found within a given measurement period (e.g., Phillips 1977, 1985; Long and Huang 1976; Donelan et al. 1985). We wish to measure the directional shape of the spectrum, not just the peak directional components, which requires rather more resolving power than that needed to see the directional peaks. To observe the crosswind wave components on an obliquely oriented sonar beam, the sensitivity required is about 100 times that needed to see the alongwind components of the same frequency travelling parallel to the beam.

An attractive shape for a sonar beam arises because of the "brightness" of the surface (or near-surface). Empirically, with winds over a couple meters per second, the backscatter from the surface zone is 30 to 40 dB (10^3 to 10^4 times) louder than the "volume backscatter" from below. For acoustic frequencies over 60 kHz or so, the backscatter at grazing angles of incidence (within 30° of parallel to the surface) appears to be due primarily to a subsurface layer of bubbles, which are extremely efficient scatterers of sound (Urick 1975; Clay and Medwin 1977; McDaniel and Gorman 1982, etc.). As a result, if any part of the beam intersects the surface bubble-layer within a given range-bin, the

Corresponding author address: Dr. Jerome A. Smith, A-013, MPL, Scripps Institution of Oceanography, La Jolla, CA 92093-0213.

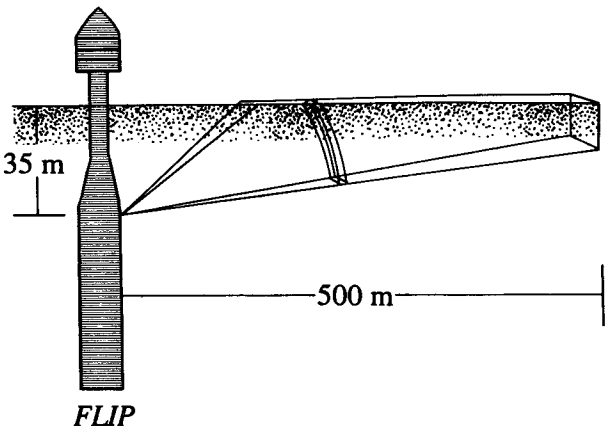

FIG. 1. A schematic view of FLIP with the fan-shaped sonar beam radiating out to 500 m. Because the backscatter from the near surface layer of bubbles (shown schematically as specks) is much brighter than that from below, the measurement can be considered to have the same one meter depth-scale as the bubbles. The intensity of the acoustic return is roughly proportional to the number of bubbles in the sample volume.

backscatter (and hence the measured Doppler shift) is completely dominated by that part. Thus, an excellent choice is a beam which is broad in the vertical plane, yet narrow in azimuth (see Fig. 1). The effective sensor location (or measurement volume) is confined vertically by the scale depth of the surface bubble layer (of order 1 m), azimuthally by the beam shape, and in range by timing. The resulting measurements are robust with respect to all platform motions other than spinning azimuthally (yaw).

For a targeted range of 500 m, a 200 kHz sonar is indicated. With a practical range resolution of 3 or 4 m, significant advances can be expected; e.g., in estimating the total energy in oppositely directed components, thought to produce low frequency pressure fluctuations detected at the sea floor, at over 4000 m depth (Longuet-Higgins 1948).

2. Sonar resolution

The sonar processing scheme considered here is as follows: (i) a sinusoidal "pulse" of duration T_p is transmitted (a single tone); (ii) the subsequently received backscatter is complex-homodyned with the same frequency (i.e., it is multiplied by a sine reference and simultaneously with a cosine reference, and each channel is low-pass filtered to form a complex "envelope function" of the return); (iii) time-lagged autocovariances are formed by averaging over time $T_a = NT_i$, where T_i is the time between samples A_n of the envelope; e.g., the lag-1 covariance is given by

$$\hat{C}_1 \equiv \frac{1}{N}\sum_{n=1}^{N} A_n A_{n-1}^{*}; \quad \text{and} \tag{1}$$

(iv) the Doppler shift of the return is estimated from the autocovariance at lag-1:

$$\hat{U} \equiv \frac{c}{2\sigma_0 T_i}\,\text{atan}\left[\frac{\text{Im}(\hat{C}_1)}{\text{Re}(\hat{C}_1)}\right], \tag{2}$$

where c is the speed of sound and σ_0 is the radian frequency of the transmitted pulse (cf., Rummler 1968; Miller and Rochwarger 1972). This is known as an "incoherent scheme" since each transmission ("ping") is treated independently, rather than forming coherent averages from ping to ping. For a uniform velocity over the averaging "cell," a lower bound on the error variance of the velocity estimate is given by

$$\text{Var}(\hat{V} - V) \equiv (\Delta V)^2 \geqslant \frac{(c/2\sigma_0)^2}{T_a[T_p - T_i - T_a(T_p - T_a)/(2T_p - T_a)]} \tag{3}$$

(see appendix A). In practice, (3) provides an optimistic but reasonable estimate of sonar performance (within a factor of 2 or 3), provided that the pulse length T_p is shorter than the "natural" decorrelation time arising from independent movements of the scatterers in the ensonified volume. For T_p longer than a few milliseconds, the scatterers can move a significant fraction of a wavelength while ensonified; this has an effect roughly equivalent to reducing T_p in (3).

The sound at the trailing edge of the moving pulse coincides with sound reflected from the leading edge at a time $\frac{1}{2}T_p$ earlier. Thus, at any instant, the received signal arises from a volume of length $\frac{1}{2}cT_p$ in range. Averaging this received signal over a time $T_a = T_p \equiv T$ gives rise to triangular "response elements" for the velocity estimates, with a base-length of cT and with independent estimates arising at range intervals of

$$\Delta R = \tfrac{1}{2}cT. \tag{4}$$

For fixed σ_0 (and c), (3) and (4) show that reducing T reduces ΔR but increases ΔV, and vice versa. In fact, the "error product" is independent of T:

$$E \equiv \Delta R \Delta V \cong c^2/4\sigma_0^2. \tag{5}$$

The simplest way to reduce E is to increase the sonar frequency σ_0. Higher frequency sound, however, is attenuated more rapidly in the ocean, so there is a tradeoff in frequency selection between total range and the error product E. Since a real sonar system is generally restricted to operate near its "design frequency" σ_0, E is an essential constant of the system.

The error product can also be reduced by "coding" the pulses. For example, a simple scheme is to transmit N different tones, each of which can be isolated by bandpass filtering. With an N-tone system, information from each tone is independent. This results in a reduction of $(\Delta V)^2$ by N^{-1}, and so reduces E by the factor $N^{-1/2}$. For present purposes, other codes can

be represented as an equivalent number of tones. (It should be noted, however, that sonar systems are ultimately limited in the peak power transmitted, because of the electronics, cavitation, or nonlinear propagation effects, as discussed below. Thus, transmitting more tones simultaneously will generally reduce the total range achievable at a given frequency.)

Given estimates of surface velocity at a large number of ranges, it is natural to consider their spatial Fourier transform. Both theory and experience suggest that the velocity estimation error variance is distributed equally among the wavenumbers (i.e., is "white noise"). Thus, let

$$(\Delta V)^2 = \int_0^{k_N} Q dk = \int_0^{\pi/\Delta R} Q dk = Q(\pi/\Delta R), \quad (6)$$

where the noise level Q is independent of k, and the "Nyquist wavenumber" is $k_N \equiv \pi/\Delta R$. Here, the choice is made to represent the "transect" of real velocity estimates as the real part arising from a spectrum with only positive wavenumbers, rather than, e.g., as conjugate pairs. This choice is made to simplify the interpretation as amplitudes of surface waves, as should shortly be more clear. Making use of (5) augmented by $N^{-1/2}$ as discussed above, we can write

$$Q = (\Delta V)^2 \Delta R/\pi = E^2/\pi\Delta R = c^4/16\pi N\sigma_0^2\Delta R. \quad (7)$$

The sonars make velocity measurements in each range interval every Δt seconds (say), so it is natural to consider frequency spectra of the resulting data. To illustrate, for each along-beam wavenumber k_x, the time-series of complex coefficients can be transformed. This yields both positive and negative frequencies, corresponding to waves propagating in either of the two directions along the beam. It is conventional to rearrange these into an array of only positive frequencies, with (+) and (−) wavenumbers denoting the two directions of propagation. (One may alternatively first form the time-frequency transforms of the velocity data at each range, choosing to represent the results as only positive frequencies. The space-wavenumber transforms of the frequency coefficients then yields a matrix of frequency-wavenumber coefficients arranged as + and − wavenumbers with only + frequencies. These coefficients are a simple rearrangement of those just described.) This rearrangement does not affect the present noise-level analysis. Again the velocity estimation noise is white, so at each k,

$$Q = \int_{-\omega_N}^{+\omega_N} \hat{Q} d\sigma = \int_{-\pi/\Delta t}^{+\pi/\Delta t} \hat{Q} d\sigma = \hat{Q}(2\pi/\Delta t), \quad (8)$$

where $\omega_N = \pi/\Delta t$ (or $f_N = 1$ cycle$/2\Delta t$) is the Nyquist frequency. Using (7), we obtain the (k_x, ω) velocity noise density,

$$\hat{Q} = Q\Delta t/2\pi = \frac{c^4\Delta t}{32\pi^2 N\sigma_0^2\Delta R}. \quad (9)$$

The estimation noise level is reduced by (i) increasing the sonar carrier frequency σ_0, (ii) decreasing Δt, (iii) increasing ΔR, or (iv) increasing N, the number of tones. Both (i) and (ii) compete directly with the maximum ranges achievable, while (iii) just restates the competition between ΔR and ΔV. Increasing N, on the other hand, merely increases the complexity of the design and analysis.

3. Range vs sample interval: dispersion

The finite speed of sound introduces a possible tradeoff between the maximum wave frequency observed and the maximum range. The maximum range (ignoring attenuation) would be

$$D = \Delta t(c/2). \quad (10)$$

Two factors help resolve the competition between the desire to increase D (by increasing Δt) or to increase f_N (by decreasing Δt). One is that attenuation of the sound limits the maximum range achievable. Another is that the maximum wavenumber, $k_N = \pi/\Delta R$, is associated with a specific wave frequency. The first of these is addressed in a later section. The second factor implies that, even if greater ranges are achievable, it may be desirable to use a shorter Δt in order to "match" the Nyquist frequency to the wavenumber resolution, or to use a larger ΔR to reduce the noise level. The linear dispersion relation for surface waves relates any wave frequency to a wavenumber magnitude, $k \equiv |\mathbf{k}|$. In deep water,

$$\omega^2 = gk. \quad (11)$$

The sonar measures only one component of $\mathbf{k}$, $k_x \leq k$. Also, at a given frequency ω, contributions from the harmonics of longer waves would have wavenumbers smaller than the "dispersive value." At any given frequency ω, then, the dispersive value of k is the maximum we need to resolve. Thus, it is natural to associate the Nyquist wavenumber with the Nyquist frequency of the system via dispersion (11). This yields

$$\Delta t = \pi/(gk_N)^{1/2} = (\pi\Delta R/g)^{1/2}. \quad (12)$$

The ability of the sonar system to measure the full frequency-wavenumber spectrum is one of its greatest attractions; hence, it would be a pity to "waste" wavenumber resolution by failing to resolve the corresponding frequencies. Also, reducing range requirements could mean less power, fewer tones, or smaller arrays, any of which reduces the cost or clumsiness of the system.

This "Nyquist matching" is used to define a "matched system," which is used as a guide in designing the sonar system. The feasibility of reaching the desired range can then be explored. For such matched systems, using 10 and 12,

$$D = (\pi \Delta R/g)^{1/2}(c/2), \quad \text{or} \tag{13}$$

$$\Delta R = 4gD^2/\pi c^2. \tag{14}$$

The spectral noise levels Q and $\hat{Q}$ are compared with estimates of the signal levels expected from surface waves at the largest wavenumbers and frequencies, k_N and ω_N (since these are the smallest signals). This allows estimation of a corresponding minimum range resolution ΔR at which one can expect to detect the surface waves.

4. Wavenumber spectra

First consider a wavenumber spectrum, as can be estimated from a single ping. In the next section, a combined frequency-wavenumber spectrum, using a series of pings from one beam, is considered. The mean square displacement of the sea surface can be described by

$$\overline{\zeta^2} = \int_{-\infty}^{\infty}\int_{-\infty}^{\infty} \psi(k_x, k_y)dk_x dk_y, \tag{15}$$

where $\overline{\zeta^2}$ is the mean-square surface displacement (elevation), and ψ is the two-dimensional wavenumber spectrum of the surface waves. An instantaneous transect of the elevation ζ in the x-direction, for example, would yield a 1-D "equilibrium spectrum,"

$$\chi(k_x) = \int_{-\infty}^{\infty} \psi(k_x, k_y)dk_y \approx Bk_x^{-3}, \tag{16}$$

(say), for k_x larger than some lower cutoff (or peak) wavenumber k_0, and where B has an observed value of about 0.004 for x aligned with the wind (e.g., see Phillips 1977, 1985). The along-wind slope spectrum then takes the form

$$S_{xx}(k_x) = \int_{-\infty}^{\infty} k_x^2\psi(k_x, k_y)dk_y \equiv k_x^2\chi(k_x) \tag{17}$$

(for wind in the x-direction). Observations of along-wind and cross-wind slopes indicate that the cross-wind slopes have about half the variance of the along-wind slopes (e.g., Long and Huang 1976). This is consistent with an angular spread at fixed k roughly proportional to $\cos^8(\phi/2)$ (as will be seen shortly). Based on this, a simple but reasonable model for the "equilibrium range" of the spectrum (i.e., for $k > k_0$) is

$$\overline{\zeta^2} = \int_{k_0}^{\infty}\int_{-\pi}^{+\pi} \beta k^{-3}\cos^8\left(\frac{1}{2}\hat{\phi}\right)d\phi dk, \tag{18}$$

where $k = |k| = (k_x^2 + k_y^2)^{-1/2}$, and where $\hat{\phi} = \phi - \phi_w$ (say) is the angle of $\mathbf{k}$ from the wind. (A $\cos^2\phi$ spectrum is often used, but it seems reasonable for the spectrum not to fall to zero at 90° off the wind; the two forms are otherwise hardly distinguishable.) An elevation transect yields a single-component wavenumber spectrum in $|k_x|$, so that

$$\overline{\zeta^2} = \int_0^{\infty} \chi(|k_x|)dk_x$$

$$= \int_{-\pi}^{\pi}\int_{k_0\cos\phi}^{\pm\infty} \beta k_x^{-3}\cos^2\phi\cos^8\left(\frac{1}{2}\hat{\phi}\right)d\phi, \tag{19}$$

where the sign of $\pm\infty$ is taken as that of $\cos\phi$. For $k_x > k_0$, the order of integration may be reversed, yielding an equilibrium range spectrum of the form

$$\chi(|k_x|) = \beta|k_x|^{-3}\int_{-\pi}^{\pi}\cos^2\phi\cos^8\left(\frac{1}{2}\hat{\phi}\right)d\phi \rightarrow$$

$$(49\pi/128)\beta k_x^{-3} \equiv Bk_x^{-3}, \tag{20}$$

where the limit is for a transect parallel to the wind, $\phi^w = 0$. For a transect perpendicular to the wind (either along the y-axis, or along x with $\phi^w = \pi/2$), $\chi(k_y) \rightarrow (21\pi/128)\beta k_y^{-3}$, which is roughly half (3/7) the along-wind value. If $B \approx 0.004$ (Phillips 1985), then (20) implies $\beta = 0.0033$.

A sonar beam provides transects of (nearly) horizontal velocity in the along-beam direction. For a linear wave field, the velocity components have the magnitude of the slope times phase-speed, $c = (g/k)^{1/2}$, so the spectral density of the velocity signal along the x-axis is $c^2k_x^2\psi = (gk_x\cos\phi)\psi$. In the equilibrium range ($k_x > k_0$):

$$V_x^2(|k_x|) = g\beta|k_x|^{-2}\int_{-\pi}^{\pi}|\cos^3\phi|$$

$$\times\cos^8\left(\frac{1}{2}\hat{\phi}\right)d\phi \rightarrow (227/210)g\beta k_x^{-2} \equiv gB^v k_x^{-2}, \tag{21}$$

where (again) the limit is for wind parallel to the beam, taken as the x-axis, so $\phi^w = 0$. Comparing (21) with (20), $B^v \approx 0.0036$. Setting $\phi^w = \pi/2$ yields the cross-wind velocity spectrum,

$$V_y^2(|k_y|) = (8/21)g\beta k_y^{-2}, \tag{22}$$

which is about 0.35 times the size of (21).

In order to form a directional estimate, each wave component must be detected by two or more beams. A wave traveling perpendicular to a sonar beam would not be detected by that beam, because such a wave produces no orbital motion parallel to the beam. Thus, for the present purpose, consider a "worst-case" beam oriented at 60° to the wave (e.g., using three beams to cover all directions). Suppose we wish to detect cross-wind components ($\hat{\phi} = 90°$) in each ping on this "worst-case" sonar beam. From the form of (21), the observable signal is reduced by $\cos^3 60° \cos^8 45° = 1/128$. To detect the wave-components perpendicular to the wind on this worst-case beam, then, requires a sensitivity about 128 times greater than that at which the downwind components would first appear in a

downwind beam. This "directional detection requirement" can be written (taking x to be along the beam)

$$Q \leqslant (g\beta/128)k_x^{-2}. \quad (23)$$

Setting $k_x = \pi/\Delta R$ and using (7), we find a lower bound on single-beam range resolution, ΔR_1, in terms of the error-product E:

$$\Delta R_1 \geqslant (128\pi E^2/g\beta)^{1/3} = (2c^4/\pi g\beta N)^{1/3} f_0^{-2/3}, \quad (24)$$

where $f_0 = \sigma_0/2\pi$ is the sonar frequency in Hz. For example, with $c = 1500$ m s^{-1}, $g = 9.8$ m s^{-1}, and $\beta = 0.0033$, a single-tone 200 kHz sonar yields $\Delta R \geqslant 14$ m or so. Note that this is required for detection of waves 90° off the wind and 60° off the sonar beam direction. (Note also that the complications of detecting such components in the presence of much larger downwind components are not addressed here.) For a beam directed parallel to the wind, dominant-directional waves should appear in data taken with resolutions down to 2.7 m.

There are several possible ways to improve on this resolution limit. For four tones ($N = 4$), the range resolution can be reduced to $\Delta R_1 = 8.6$ m; for $N = 16$, 5.4 m resolution is achievable. If the beam separations are reduced to 45° (e.g., using four beams instead of three), the tolerable velocity error is increased by $2^{3/2}$. Alternatively, if the sonar system can be steered relative to the wind, the weak 90° components could be aligned with a more sensitive axis of the array. For example, putting two beams within 30° of the 90°-to-the-wind direction increases the effective sensitivity by $3^{3/2}$ without necessarily increasing the number of beams. (A steered system also has the potential for "quieting down" the dominant-directional waves, by aligning them with an insensitive axis of the array. This would effectively "prewhiten" the measurements with respect to direction.) Finally, one can use information from more than one "transect" (ping), forming two-dimensional (k_x, ω) spectra from the data.

5. Wavenumber-frequency spectra

If the surface wavefield roughly obeys the linear dispersion relation, then a given frequency corresponds also to a fixed wavenumber magnitude, $k = \omega^2/g$. Using the spectral form given by (18), the mean square value of the x-component of the surface-wave orbital velocities (i.e., the signal power) is

$$\langle U_x^2 \rangle = \iint (c^2k_x^2)\beta k^{-3} \cos^8\left(\frac{1}{2}\hat{\phi}\right) dk d\phi$$

$$= \iint 2\beta g^2\omega^{-3} \cos^2\phi \cos^8\left(\frac{1}{2}\hat{\phi}\right) d\omega d\phi. \quad (25)$$

Discrete time–space transforms of the velocity data yield estimates at discrete (ω, k_x) locations, within $\Delta\omega$, Δk_x bands. On the (k, ϕ) plane, these are intersections of circles (constant k) and lines (constant $k_x = k\cos\phi$; see Fig. 2). The transformation of ϕ to k_x (with k or ω fixed) yields

$$dk_x = kd(\cos\phi) = -(\omega^2/g)\sin\phi d\phi, \text{ or}$$

$$d\phi = \frac{-gdk_x}{\omega^2 \sin\phi}, \quad (26)$$

which is singular along the x-axis, $\phi = 0$ (or $n\pi$). The singularity is integrable, however, so that a finite FFT produces finite estimates (see Fig. 2). The result is left most conveniently in terms of frequency, ω, and direction, $\phi = \arccos(gk_x/\omega^2)$:

$$\langle U_x^2 \rangle = \int_{-\infty}^{\infty} \int_{-K}^{K} \hat{V}_x^2(\omega, k_x) dk_x d\omega, \quad \text{where} \quad (27)$$

$$\hat{V}_x^2(\omega, k_x) \equiv 2\beta g^3\omega^{-5} \cos^8\left(\frac{1}{2}\hat{\phi}\right) \cos^2\phi/\sin\phi,$$

$$\text{if} \quad |\omega| > \omega_0, \quad \text{or}$$

$$\equiv 0, \text{ otherwise}, \quad (28)$$

where $K \equiv \omega^2/g$ and ω_0 corresponds to k_0, the "peak frequency" wave. For each value of ω and k_x there are two possible values for k_y, corresponding to $\pm\phi$ (see Fig. 2). Although both $\pm k_y$ contribute to $\hat{V}_x^2(\omega, k_x)$, they are kept separate here, since ultimately we wish to disentangle them using information from more than

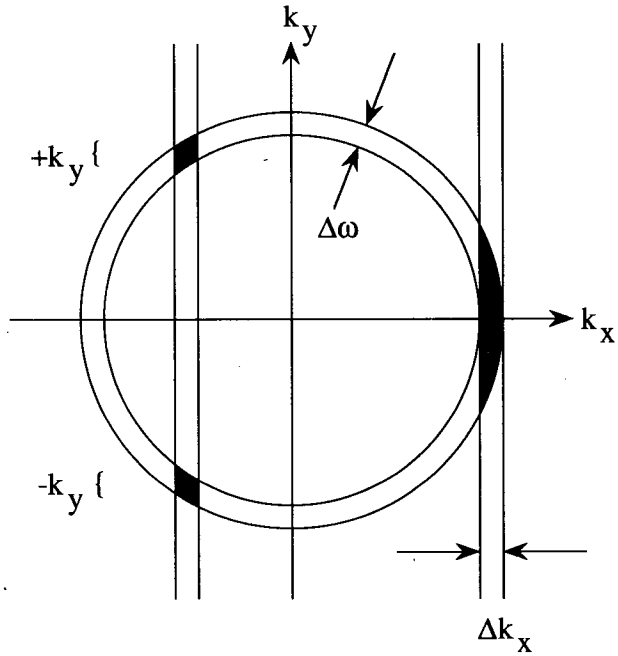

FIG. 2. Schematic view of the area in the (k_x, k_y) plane included in a $\Delta\omega - \Delta k_x$ cell of a single-beam finite Fourier transform. Contributions arise from both + and − k_y intervals (as shown on the left). For wave components parallel to the beam, the nonfinite transform becomes singular; for the finite case, a somewhat large but finite area is included near the k_x axis (dark area shown on the right).

one beam. Conceptually, this can be accomplished in (27) by allowing $\pm\omega$ in $\hat{V}_x^2(\omega, k_x)$, and taking $k_y > 0$ for $\omega > 0$ and $k_y < 0$ for $\omega < 0$.

We now apply the same worst-case criteria as above: let $\hat{\phi} = 90°$, $\phi = 60°$, and $\omega = \omega_N = (gk_N)^{1/2} = (g\pi/\Delta R)^{1/2}$ to assess the weakest velocity signal to be discerned from the Doppler estimation noise, $\hat{Q}$:

$$(\hat{V}_x^2)^{\min} = 2^{-4}3^{-1/2}\pi^{-5/2}g^{1/2}\beta\Delta R^{5/2}. \quad (29)$$

From (9) and (10), and with $f_0 = \sigma_0/2\pi$,

$$\hat{Q} \approx \frac{2^{-6}\pi^{-4}c^3D}{Nf_0^2\Delta R}. \quad (30)$$

Requiring $\hat{Q} \leq V_x^2$ yields

$$(\Delta R)^7 \geq \frac{(3/16\pi^3)D^2c^6}{\beta^2gN^2f_0^4}, \quad (31)$$

which is useful when the sound at frequency f_0 is limited by attenuation in reaching D. For a matched system, ΔR and D are related by (13). The resulting simplified form, ΔR_2, is directly proportional to ΔR_1 from the 1-D case:

$$(\Delta R_2)^3 = (3^{1/2}/8\pi)(c^4/g\beta Nf_0^2) = (3^{1/2}/16)(\Delta R_1)^3. \quad (32)$$

For example, at 200 kHz, the minimal ΔR_2 is 6.5 m (with one tone, etc., as before). Steering so two beams are within 30° of the crosswind direction would reduce this to about 3.75 m. The improvement in ΔR_2 over ΔR_1 can be compared to an equivalent number of tones: $N^e = 16/3^{1/2} \approx 9$.

In practice, attenuation (etc.) can limit the maximum range attainable to something less than the "matched value" for a single-tone system. From (31), however, the minimal ΔR depends on D only as $D^{1/2}$, so that using an "unmatched" total range D (e.g., increasing the sample rate in time) won't change the range resolution limit much from ΔR_2, as given by (32). In other words, ΔR depends more strongly on, e.g., the acoustic frequency f_0 than on the sample interval between pings, Δt. To estimate the maximum range attainable, (32) gives a reasonable value for ΔR (and hence T). Using the values given above for B^v, c, and g, (24) and (32) can be evaluated as

$$\Delta R_1 \approx (46400)f_0^{-2/3} \quad \text{and}$$

$$\Delta R_2 \approx (22100)f_0^{-2/3}. \quad (33)$$

(with $c = 1500$ m s^{-1}, $g = 9.8$ m s^{-2}, $\beta = 0.0033$, and $N = 1$). Note that the improvement in ΔR_2 over ΔR_1 depends on the signal being stationary over the observation interval. In addition, a longer time series would allow the frequency to be "overresolved" compared to the wavenumber resolution, so that extra degrees of freedom could be obtained by averaging. The surface wave field evolves slowly in time, however, so that the increase in degrees of freedom must be balanced against the less tangible errors incurred because of nonstationarity.

Given the additional accuracy and range resolution obtained by including the frequency information as well as wavenumber from one sonar beam, it is natural to ask what further benefit can be obtained by including other beams to form a 3-D spectrum. Will this further reduce the minimum advisable range resolution? Probably not. Unlike the above spectral forms, the 3-D spectrum is vastly underdetermined from any reasonable number of sonar beams. Thus, all available information (or degrees of freedom) may be required to limit aliasing.

6. Maximum range versus sonar frequency

For a given sonar frequency, there is an absolute maximum range from which a Doppler signal can be recovered from the backscatter. This arises because (i) the effective transmission intensity is limited either by "cavitation" at the transducer face, or by nonlinear propagation effects ("saturation"); (ii) the sound is attenuated with range; and (iii) there are finite levels of ambient noise. For frequencies greater than a few kHz, this range limitation is significant. In the following sections, the factors limiting total achievable range as a function of acoustic frequency are reviewed in some detail.

A sensible way to proceed is to select a desired maximum range, based on the longest waves to be resolved, and then determine the highest acoustic frequency at which a Doppler signal can be recovered out to that range. In the Pacific, swell sometimes attains periods of 18 seconds, corresponding to 500 m wavelengths. More commonly, there is 10–12 second swell, and fully-developed "local" seas which attain periods of 8 or 9 seconds. These have wavelengths around 100 to 200 m. Thus, it appears reasonable to set $D = 500$ m to resolve even the long swell, while the more commonly observed swell and seas can be measured with more precision. This corresponds to a 2/3 second interval between pings, or a Nyquist period of 4/3 seconds. Matching the Nyquist wavenumber and frequency via surface wave dispersion implies (from 14) that $\Delta R = 1.4$ m for $D = 500$ m. Can this combination be achieved?

Note that aliasing of energy from smaller waves (larger wavenumbers or frequencies) should not be a problem. The inherent (triangular) spatial averaging of the sonar systems helps filter out energy from higher wavenumbers (and hence frequencies), which is already reduced because of the steep spectral slope associated with surface waves.

7. Beam geometry

As mentioned in the introduction, it is useful to have an idealized beam geometry in mind. First, let the ideal

beam be defined by two angles in polar spherical coordinates, then let the pole be horizontal, so the equator lies in the vertical plane of the "fan-shaped" beam. The generous vertical spread of the beam is delimited by θ, corresponding to the "longitudinal" angle along the "equator"; the narrow horizontal spread of the beam is delimited by ϕ, spanning the equator equally (from "latitude" $-\phi/2$ to $+\phi/2$). The cross-sectional area of the beam at radius r is then

$$A(r) = r^2\theta(2\sin\phi/2) \approx r^2\theta\phi. \qquad (34)$$

Note that only $\phi/2$ need be small in the approximation; θ may be 2π (corresponding to a cylindrical array).

A good model array is a bar, with horizontal dimension d_x and vertical dimension d_z (say). These can be determined in terms of θ, ϕ, and the acoustic frequency f:

$$d_x = \lambda/(2\sin(\phi/2)) \approx \lambda/\phi = c/f\phi, \quad \text{and}$$

$$d_z = \lambda/(2\sin(\theta/2)) \approx \lambda/\theta = c/f\theta, \qquad (35)$$

where $\lambda = c/f$ is the wavelength of the sound. The approximations are reasonable for θ and ϕ up to about 1 radian (or 60°), and is sufficient for the present use.

8. Attenuation

There are two components to the attenuation of backscattered signal with range: (i) geometric spreading of the beam and backscatter, and (ii) absorption in the water (primarily by $MgSO_4$ "relaxation" in the ocean, but also by bubbles near the surface). The outgoing beam spreads spherically, yielding an r^{-2} factor in the intensity (where r is range). The backscattered sound also spreads spherically, making it r^{-4}. For surface scattering, the backscattered intensity is proportional to the surface area ensonified, or to approximately $r\phi\Delta R$, where ϕ is the azimuthal spreading angle of the outgoing beam (as defined above). Thus, so far we have

$$I \propto I_0 r^{-3} s_s \phi \Delta R, \qquad (36)$$

where, following conventional notation, I_0 is the outgoing intensity at a nominal range of 1 m, and s_s is the ratio of backscattered intensity per m^2 of surface (at nominally 1 m from the centroid of the area) to the incident intensity. The "backscattering strength" s_s is a function of wind, acoustic frequency, and incident angle, but is assumed to be roughly constant in range (on the average). For typical oceanic conditions (moderate winds), the total "cross section" related to s_s is small, so the "shading" of distant scatterers by near ones is neglected in (36). Also, since the sonar beam is incident from a few degrees below the surface, sound reaching the farther ranges passes below the near-surface bubble layer at the closer ranges.

Absorption (e.g., by $MgSO_4$) is often more important than spreading. Absorption is well modeled by exponential decay, so that (with two-way travel over range r):

$$I(r) \approx (I_0 s_s \phi \Delta R) r^{-3} e^{-2Ar}, \qquad (37)$$

where A is the fraction of sound intensity absorbed per unit distance in range, r. The intensity equations are conventionally cast in terms of dB, say L (dB) $\equiv 10 \times \log_{10} I$, so that (37) becomes

$$L(r) = L_0 + S_s - 2\alpha r - 30\log_{10} r + 10\log_{10}(\phi\Delta R), \qquad (38)$$

where all distances are in m, $L_0 \equiv 10\log_{10} I_0$, $S_s \equiv 10 \times \log_{10} s_s$, and $\alpha \equiv (10\log_{10} e)A$. Figure 3 shows an empirical fit to α (in dB per meter) vs sonar frequency in seawater under fairly typical conditions (Fisher and Simmons 1977).

9. Backscattering strength

The backscattering strength at the surface of the oceans varies with wind, sonar frequency, and incident angle. Here, we need only consider angles approaching grazing incidence, say less than 30° (see Fig. 4). Sonar observations using 60 kHz and higher frequencies at near-grazing angles are consistent with scattering from a near-surface layer of bubbles (Urick 1975; McDaniels and Gorman 1982). Observations of near-surface bubbles indicate an exponential decay in number of

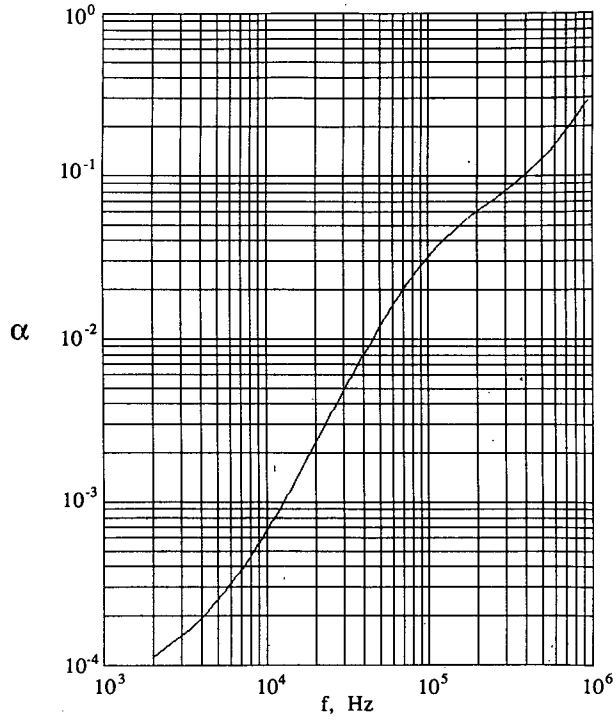

FIG. 3. Attenuation α (in dB m^{-1}) vs acoustic frequency f (Hz), in seawater of 35 ppt salinity, 15°C, 1 atm pressure, and pH = 8. (From the formulae given by Fisher and Simmons 1977).

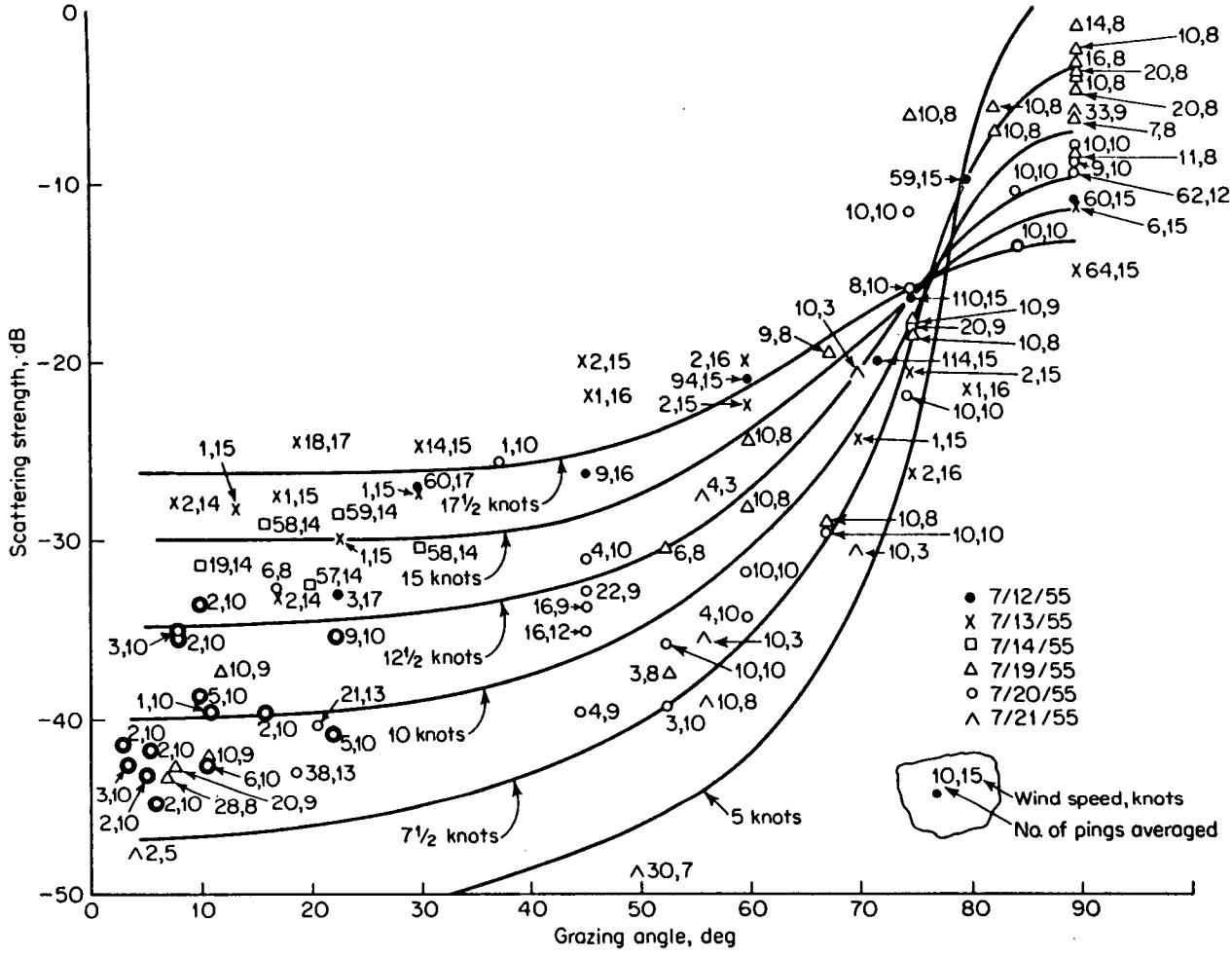

FIG. 4. Variation of sea-surface scattering strength at 60 kHz with angle at different wind speeds off Key West, Florida. Plotted points show the number of pulses averaged and the wind speed (in knots) for individual determinations. Extra bold circles, near the lower left-hand corner, flag the measurements for 5 m s^{-1} winds (10 knots) and angles less than 30° (from Urick 1975).

bubbles with depth, with e-folding scales of order 1 m (Thorpe 1986; Crawford and Farmer 1987; Walsh and Mulhern 1987). Also, the number of bubbles per m^3 at a fixed depth increases roughly in proportion to W^3, where W is the windspeed (Crawford and Farmer 1987; Walsh and Mulhearn 1987).

Bubbles are efficient scatterers because they can resonate by oscillating radially. The frequency-dependence of the scattering intensity from bubbles thus depends on the bubble spectrum. Above some cutoff frequency, the scattering level should become roughly constant, proportional to the total surface area of all bubbles. The location of this "cutoff" is not well known at present. Measurements at 60 and 119 kHz both indicate a backscattering strength S_s of about −40 dB under 5 m s^{-1} winds (see appendix B). Assuming that the strength doesn't vary much over 60 kHz, but retaining the W^3 wind dependence,

$$S_s \approx -40 \text{ dB} + 30 \log(W_*), \qquad (39)$$

where $W_* = W/(5 \text{ m s}^{-1})$. It should be noted that S_s may decrease more rapidly than indicated here as W drops below 3 or 4 m s^{-1}, when whitecaps are absent.

10. Source level limits

Two effects can limit the intensity of sound arriving at some distance from the source: (i) For large pressure fluctuations, bubbles can form spontaneously near the transducer face (cavitation). Once this occurs, additional energy simply causes more bubbles to form rather than increasing the sound intensity. (ii) As the sound propagates away from the source, nonlinear effects cause the pressure variations to evolve into "shock fronts," which dissipate energy rapidly. Both cavitation and saturation are strongly amplitude dependent, and so operate preferentially on the main lobe of the beam pattern. Either would cause side-lobe interference to increase. It is therefore desirable to operate the sonars with transmission amplitudes small enough to avoid

either the formation of shock fronts or cavitation. Here, we first investigate the cavitation limit, and then compare it to the "saturation limit" as described by Shooter, Muir, and Blackstock (1974). (Electronic limitations are neglected here in view of their mercurial nature.)

So far we have considered intensity relative to a source level, L_0. Ultimately, the returned intensity $L(r)$ will be compared to the ambient noise level, L_N, to find the range at which the signal drops into the noise. Both L_0 and L_N must be in comparable units of intensity. The standard reference intensity corresponds to an rms pressure P_R of 1 μPa = 10^{-11} atmospheres (atm). Then $L_R \equiv 10 \log I_R \equiv 20 \log P_R$, so conversion from P in rms atmospheres to "standard intensity" is given by $L = 20 \log P + 220$ dB.

a. Cavitation

The intensity at which cavitation begins, $I_c \propto P_c^2$, is conveniently expressed with the rms pressure P_c in atmospheres; thus let

$$L_c = 20 \log_{10} P_c \text{ (atm)} + 220 \text{ dB re 1 } \mu\text{Pa}. \quad (40)$$

The limiting pressure P_c is a function of both frequency and depth (i.e., ambient pressure). Figure 5 shows P_c vs f at 1 atm pressure. The solid curve is given by

$$P_c = 1 + (d/10 \text{ m}) + (f/36 \text{ kHz})^2, \quad (41)$$

with d (depth) = 0. The hydrostatic pressure (d/10 m) is simply added to P_c (Urick 1975). Near the surface, and for $f > 60$ kHz or so, the last term of (41) dominates, so

$$L_c \rightarrow 40 \log f \text{ (Hz)} + 38 \text{ dB re 1 } \mu\text{Pa}. \quad (42)$$

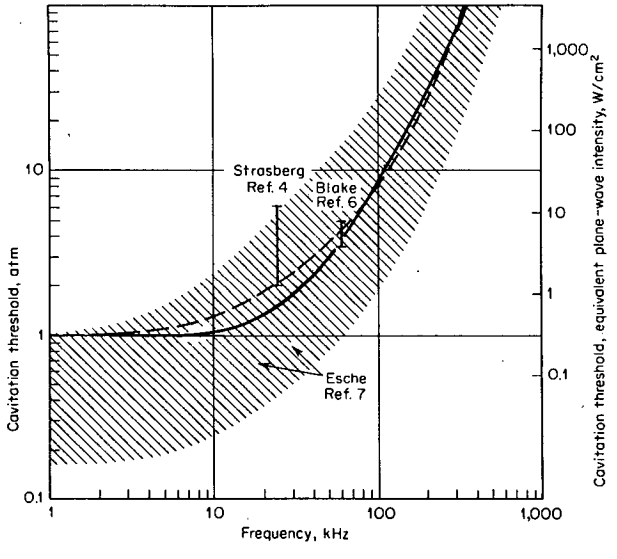

FIG. 5. Frequency dependence of the cavitation threshold. The data (from fresh water at 1 atm) are contained in the shaded area. The dashed line is a subjectively estimated average (from Urick 1975). The solid line shows the relation given in the text here (equally subjective in derivation).

For example, at 200 kHz, the last term alone yields $P_c \approx 31$ atm. Adding 2 or 3 atm increases I_c by about 10%, adding only ½ dB to L_c.

Note that the mixed layer of the ocean can be supersaturated, and is often already full of bubbles, either of which could reduce the amplitude at the onset of cavitation (when bubbles are present, they can grow by a "rectified response" to the pressure variations, which is also an effective means for absorbing sound). The shading in Fig. 5 represents a range of rms sound pressures over which cavitation is observed. The lower edge of this shaded region is a factor of 4 or 5 below the line given by (42), or 12 to 14 dB below in intensity.

The cavitation limit applies near the face of the sonar array (neglecting focusing), whereas I_C (say) is an equivalent intensity at 1 m range in the idealized beam. Converting I_c to I_C (or L_c to L_C) requires a geometric correction. Given the area of the array face, A^T, and since the total power IA is (conceptually) conserved, the equivalent intensity at 1 m in the idealized beam is

$$I_C = I_c A^T / A \text{ (1 m)} = I_c A^T / (1 \text{ m})^2 \phi\theta \quad (43)$$

$$\approx I_c(\lambda^2/\phi^2\theta^2) = I_c(c^2/\phi^2\theta^2 f^2), \quad (44)$$

where λ is in meters, c in m s^{-1}, f in Hz, and ϕ, θ are in radians. In dB, the cavitation limited source intensity L_C is

$$L_C = 220 + 20 \log(cP_c/\phi\theta f)$$

$$= 284 \text{ dB re 1 } \mu\text{Pa} + 20 \log P_c - 20 \log f - 20 \log(\phi\theta), \quad (45)$$

where $c = 1500$ m s^{-1} was used.

b. Saturation

For finite-amplitude sound waves, nonlinear effects can bring about the formation of shock fronts, which also dissipate energy rapidly (Shooter et al. 1974; Clay and Medwin 1977; see Fig. 6). As the waves spread spherically and attenuate, these finite amplitude effects eventually decrease in relative importance until essentially "linear behavior" is restored. At a given frequency and source strength, the tendency to form shocks can be characterized by "r_s", the distance at which shock waves first form, and "r_L", the distance at which the linear and nonlinear attenuation are again equal, and hence beyond which "linear behavior" is restored. For source levels less than or equal to that at which $r_L = r_s$, the formation of shocks (and hence rapid nonlinear attenuation) is presumably avoided. A maximum recommended source amplitude (leaving the beam pattern nearly unmodified) is thus described by this condition. Using the equations given by Shooter et al. (1974), and correcting for beam geometry, the equivalent source intensity satisfying this condition is

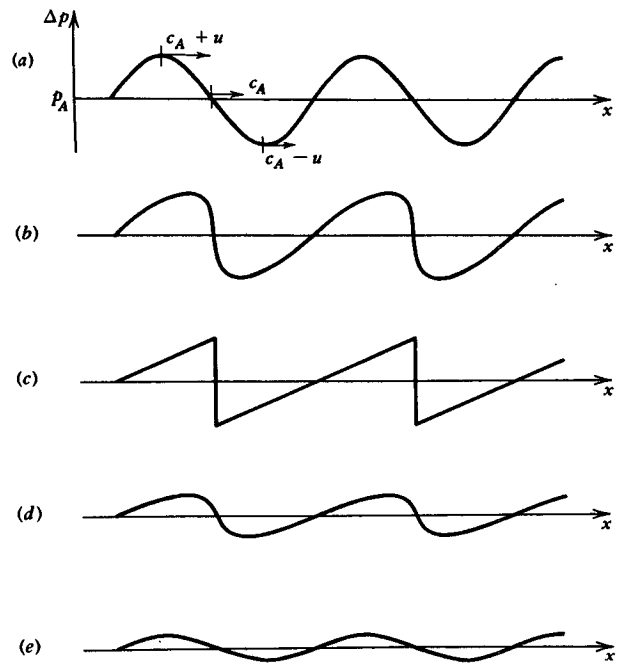

FIG. 6. Various stages in the evolution of a finite amplitude acoustic wave. The source is assumed sinusoidal. (a) Finite amplitude, nearly sinusoidal wave close to the source. (b) Somewhat distorted waveform at some distance from the source. (c) Fully developed shock wave, farther from the source. (d) "Aging" shock wave, where the attenuation of the higher frequency harmonics is faster than the transfer from the fundamental frequency. (e) Infinitesimal amplitude, degenerated shock wave (return to "linear attenuation"). From Clay and Medwin, 1977.

$$L_S = 220 \text{ dB re } 1\ \mu\text{Pa} + 20 \log P_S, \qquad (46)$$

where P_S is evaluated in appendix C.

The maximum practical source level is just the smaller of the limits set by cavitation, L_C, or by saturation, L_S (see Fig. 7). In the frequency range and for the array geometries considered here, the saturation limit dominates.

11. Ambient noise

There are several potential sources of ambient noise in the ocean, and different sources tend to dominate in each of several frequency bands (see Fig. 8). Near 100 kHz, there is an overall minimum between wind-generated noise (decreasing as f^{-2} and dominating from about 200 Hz to 100 kHz) and thermal noise (which increases as f^2 and dominates above 100 kHz). In addition, a major portion of the wind-noise is directed within about 30° to 40° of vertical (downward), so that it may be reduced by confining the beam geometry below 50° up from horizontal (for example). The wind and thermal noises have spectral densities of

$$H_W \approx 25 - 20 \log f_* + 20 \log W_*, \quad \text{and}$$

$$H_T \approx 25 + 20 \log f_*, \qquad (47)$$

in units of dB re 1 μPa per Hz, with $f_* \equiv f/100$ kHz, and $W_* \equiv W/5$ m s^{-1} (Urick 1975; Clay and Medwin 1977). Of the total noise, only the fraction within the viewing angle of the beam is accepted. For the present purpose, we take this fraction to be roughly $\theta\phi/4\pi$ for both the thermal and wind components. (In fact, the wind-noise depends on the orientation of the beam, especially in the vertical. For a beam aimed roughly horizontally, this approximation should be good to within a few dB, well within the present tolerances.) For small noise bandwidth, $B \ll f$, the combined noise intensity can be written

$$L_n = 10 \log I_n, \quad \text{where}$$

$$I_n \approx B(\phi\theta/4\pi)(10^{2.5})(f_*^2 + W_*^2 f_*^{-2}). \qquad (48)$$

(It is hoped that the use of B for bandwidth here will not be confused with the spectral constant B used previously.)

What is the admitted noise bandwidth B? This fairly complex question is addressed in appendix D. Briefly, with covariance estimates $\hat{C}_1$ formed as in (1), the sample error variance is affected by both the input filter bandwidth b and the averaging time of the received signal T. The amount of noise admitted corresponds to a bandwidth of $B = (b/T)^{1/2}$. T is found from (4) using ΔR from, e.g., (33). To choose a minimal value for b (the input filtering bandwidth), the maximum Doppler shift must be anticipated, and added to the signal bandwidth, $1/T$. For the open ocean, values

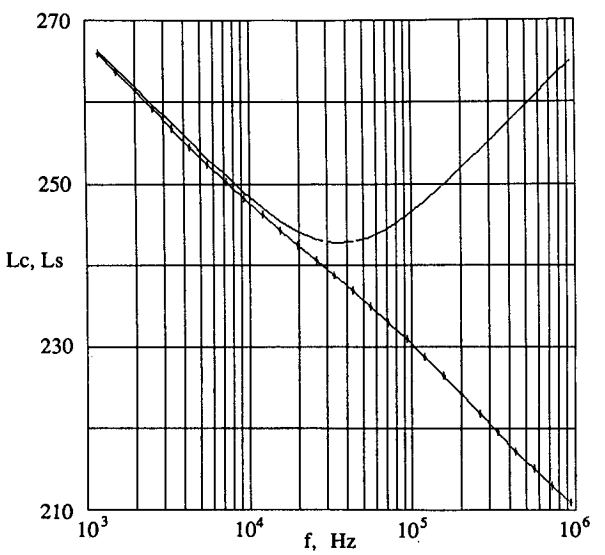

FIG. 7. The geometrically corrected "equivalent source intensity" (at 1 m in the idealized beam), at the cavitation threshold (upper, solid line) and for the "barely saturated" limit (lower, hatched line). A 30° by ⅔° beam is assumed.

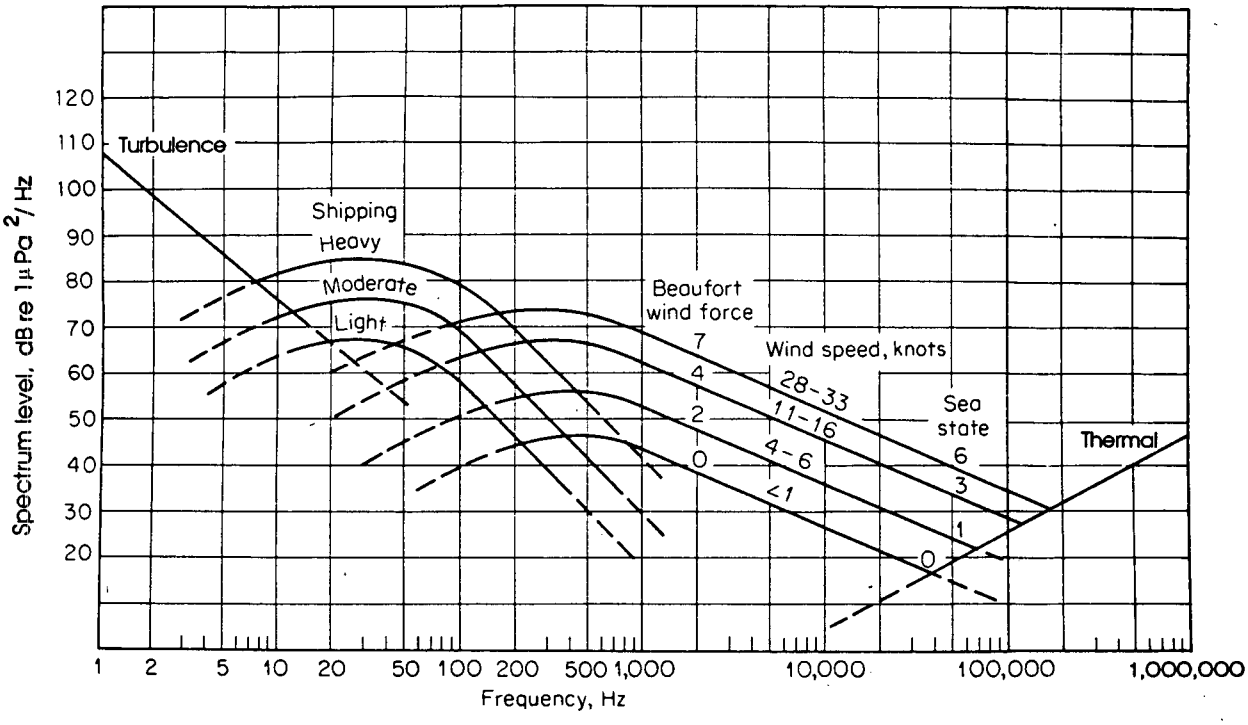

FIG. 8. Average deep-water ambient noise spectra, dB/Hz, vs frequency, Hz (from Urick 1975). The acoustic frequencies of interest here are around 100–200 kHz, near the minimum. Note also that wind-generated noise is directionally anisotropic (being louder from above than from the side) while thermal noise is inherently isotropic.

corresponding to velocities $v^{\max} = 1.5$ to 2 m s^{-1} are appropriate, owing to the surface wave orbital velocities of that magnitude. Allowing + and − velocities, the net bandwidth requirement becomes

$$b \geq T^{-1} + f_0(4v^{\max}/c). \tag{49}$$

12. Maximum range

The maximum practical range vs acoustic frequency f is found by setting $L(r) - L_n$ to a "threshold value" for the signal-to-noise ratio (S/N) in dB. Figure 9 shows the results for signal-to-noise cutoff ratios of 1 (0 dB) and 10 (10 dB), using a bar producing a 30° by ⅔° beam (roughly 1 cm by 50 cm at 200 kHz). In practice, the 10 dB cutoff is appropriate: the covariance estimation technique is nonlinear, and performance deteriorates rapidly when the signal to noise ratio falls below 10 dB. Other values employed are $W = 5$ m s^{-1}, $v^m = 1.8$ m s^{-1}, and the values given in the sections on surface wave spectra and attenuation.

With multiple tones, the signal-to-noise ratio of each must be considered independently. Since the total output power is limited by saturation or cavitation (or by the electronics), this implies that when the tones are superimposed (as, for example, in a coded pulse scheme), the power in each tone is effectively reduced. As a result, the total range is reduced by a corresponding amount. To illustrate, with ten tones superimposed, each is effectively reduced by (at least) 10 dB. The resulting range limit would lie (at least) as far below the 10 dB line in Fig. 9 as the latter lies below the 0 dB line. In contrast, a sequence of separate tones allows each to have the limiting power level.

Finally, it is useful to compare the "matched resolution," corresponding to this maximum range via (14), with the "practical resolution" resulting from comparison of the signal level vs Doppler estimation noise, embodied in (33) (see Fig. 10).

13. Summary

To summarize: (i) A lower bound for the error product $E = \Delta V \Delta R$ of the sonar system was estimated. (ii) The magnitude of the velocity noise level Q over **k**-space from a single ping (for a given ΔR) was described (a white noise level). (iii) The corresponding (white) noise spectral level $\hat{Q}$ over (ω, k)-space from a time-series of pings was evaluated in terms of acoustic frequency f_0, range resolution ΔR, sample interval Δt, and the number of tones N. (iv) A matching of total range D, wave frequency resolution ω_N, and range resolution ΔR was introduced, arising from the finite speed of sound, c, along with surface wave dispersion, $\omega^2 = gk$. Use of this matched resolution allows the expression for the 2-D noise level $\hat{Q}$ to be simplified. (v) Next, the wavenumber spectrum of surface wave velocity, as it would appear in a single sonar ping, was estimated using a simple model of the complete direc-

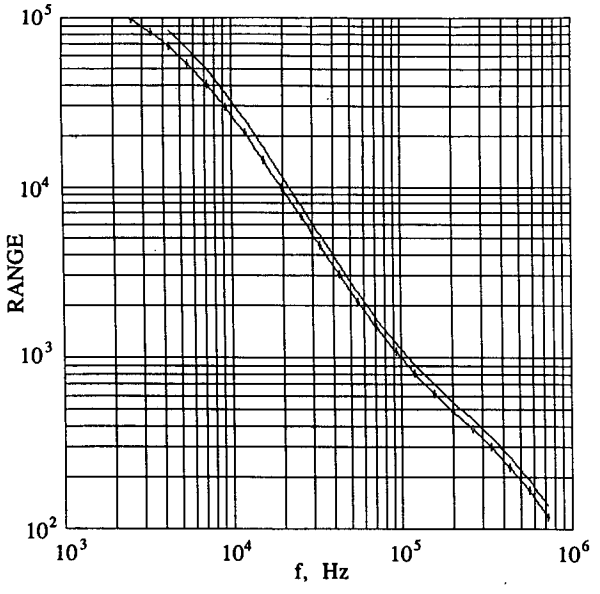

FIG. 9. Maximum range (in meters) vs acoustic frequency, as determined from saturation, attenuation, and ambient noise levels for the given beam geometry (30° vertical by ⅔° horizontal beam widths). Solid line: 0 dB signal-to-noise limit. Hatched line: range at which there remains 10 dB of signal-to-noise. In general, the 10 dB limit is more appropriate.

tional spectrum. The spectral level of wave velocity parallel to a sonar beam, $V_x^2(k_x)$, was compared with the 1-D noise level Q to determine the sensitivity needed to see the Nyquist components, $V_x^2(k_N)$, in each ping. The result was cast in terms of the minimum range resolution, ΔR_1, for which the signal from crosswind wave components is resolvable: $\Delta R_1 \propto (Nf_0^2)^{-1/3}$. (vi) The single-beam frequency-wavenumber spectrum, $\hat{V}_x^2(\omega, k_x)$, was similarly estimated and compared with the 2-D noise level $\hat{Q}$ to assess the requirement for detecting a crosswind wave component with a worst-case sonar beam from a series of pings. This yields $\Delta R_2 \propto (D/Nf_0^2)^{2/7}$. Using the matched values relating D and ΔR yields a simplified relation for the matched range resolution limit, $\Delta R_2{}^M$: $\Delta R_2{}^M \propto (Nf_0^2)^{-1/3} \propto \Delta R_1$. Further, since D only enters as $D^{2/7}$, the actual value of ΔR_2 at a given frequency will generally be close to $\Delta R_2{}^M$. For the spectral model used, $\Delta R_2{}^M$ is about half the size of ΔR_1, an improvement equivalent to using more than 9 times the number of tones. (vii) Finally, the factors limiting the total range achievable as a function of acoustic frequency f_0 were reviewed: attenuation, backscattering strength, cavitation, saturation, and ambient noise level. Of these, three emerge as the most significant over the frequency range of interest (60 kHz to 1 MHz or so): saturation (or nonlinear absorption), which limits the effective source intensity of the transmitted tone; absorption, which dominates over spherical spreading in attenuation of the intensity as the sound travels; and the ambient noise level, into which the signal ultimately drops.

14. Discussion and conclusions

A surface scanning Doppler sonar system of about 200 kHz center frequency appears to be most suitable for measuring surface waves. A total range of about 500 m permits directional estimates of typical swell and wind-generated peak waves. Resolution in range down to a few meters is commensurate with the typical horizontal and vertical scales of bubble clouds, which are the most likely "targets" responsible for scattering the sound. Balancing the Doppler estimate error vs the surface wave spectral levels in the crosswind components leads to a "practical" limit on range resolution: At 200 kHz, with a single tone and with a 60° worst-case beam orientation, this limit is about 6.5 m. A steered system with beams aimed near the crosswind direction would resolve the weaker crosswind components better, allowing range resolution down to 3.75 m (using two beams each within 30° of the crosswind direction). The practical resolution varies with the (effective) number of tones as $N^{-1/3}$, so the steered system provides an improvement equivalent to using about 5 times as many tones as the unsteered system.

For a total range of 500 m, the corresponding Nyquist matched range resolution would be 1.4 m. To

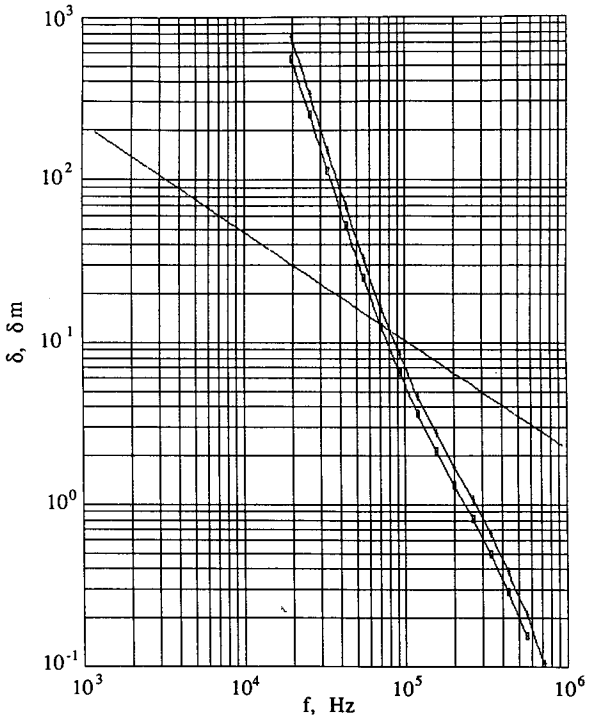

FIG. 10. Minimum range resolution from balancing estimate noise vs spectral "signal" levels (δ, plain line), and the "matched resolution" corresponding to the maximum range vs frequency as shown in Fig. 9 (δ_m; pluses: 0 dB limit; rectangles: 10 dB limit). For acoustic frequencies less than about 70 kHz, the matched resolution is achievable with the single tone system explored here. At higher frequencies, there is a gap between the matched and practical range resolutions. Multitone or coded systems may be able to close this gap.

achieve 1.4 m resolution, even with a steered system, would require an additional improvement equivalent to about 20 tones. In practice, the number of tones is limited by the hardware and electronics to rather less than 20. Coding techniques are presently being researched, to evaluate whether they can usefully achieve this resolution. In any case, with 4 (equivalent) tones the resolution can be pushed to 2.4 m, and 8 tones would allow 1.9 m resolution, a noticeable improvement. Also, note that the 1 m depth scale of the bubble layer implies that interpretation becomes tricky for surface wavelengths less than about 6 m; hence 3 m resolution may be a sensible environmentally imposed limit.

The system described allows estimation of full directional spectra (with no 180° ambiguity) over about two orders of magnitude in wavenumber k, or (equivalently) four orders in frequency. The total range in k can be increased significantly with a "nested system": two different frequencies can be used together, with some overlap in range vs resolution. Perhaps the one meter depth scale of the bubble clouds poses a limit on the small scale resolution of surface waves. Nothing prevents using an additional lower frequency system to increase the total range, though. We (myself and R. Pinkel of MPL) are developing both 200 kHz and 75 kHz systems for use on the sea surface. Preliminary results from tests at sea verify that the 200 kHz system can achieve a range of 500 m with resolution down to about 3 m (using a single tone), while the 75 kHz system reaches to 1500 m with 12 m resolution. The combined system covers nearly three orders of magnitude in k.

For the systems described, the intensity of the acoustic backscatter is a measure of the bubble population within the sample volume. By mapping both velocity and intensity down to the 1 or 2 m scale of the bubble patches, it may be possible to investigate the "life cycle" of the bubbles, from formation under breaking waves to subduction and dissolution as the currents advect them. Although no information is obtained about the vertical distribution of the bubbles, significant advances should be possible in the characterization of horizontal variation and evolution of the bubble clouds, and in relating these to the surface waves and currents.

Because velocity is the primary measurement, the mean or background currents can be estimated as well as the surface waves. Indeed, the original motivation for developing a Doppler acoustic system for use in the ocean was to investigate internal waves (e.g., Pinkel 1981), and the motivation for aiming one along the underside of the surface was to investigate mixed layer motions such as Langmuir circulation (e.g., Smith et al. 1987). Doppler sonar systems offer tremendous potential for the investigation of interactions between these motions and surface waves. Thus, although surface waves provide a good "conceptual tool" for the design of a surface scanning Doppler system, as outlined here, it is important to consider also the time and space scales of these other motions of interest. As described by Smith et al. (1987), for example, Langmuir circulation appears at all (measured) scales smaller than about three times the mixed layer depth in the crosswind direction, and are roughly 10 times longer in the alongwind direction. Thus, the nested system mentioned above can provide both the large scale information needed to characterize the alongwind scales, and the small scale information needed to investigate both the initial growth (thought to occur first at the smaller scales) and the coexistence of large and small scale circulation (how small?) later on.

Acknowledgments. This research is supported by the Office of Naval Research. The author offers thanks to Rob Pinkel for many useful and insightful discussions, and to Eric Slater for pointing out and discussing the nonlinear saturation work of Shooter et al. Thanks are also due to Mike Goldin, Lloyd Green, Steve Beck, Efird DeWitt, and the crew of FLIP for their help in developing and deploying the sonar systems.

APPENDIX A

Variance of the Doppler Estimate

The following describes a "Cramer-Rao" lower bound on the variance of the Doppler frequency estimate. It is patterned after the analysis of Theriault (1986), modified to consider discrete sampling of a bandpassed process (with sample interval T_i), and to consider an averaging time T_a not necessarily equal to the transmitted pulse length T_p.

Suppose that, after transmitting a sound pulse of duration T_p, the received signal + noise is bandpassed with a filter of width b (Hz). Then a segment of duration T_a of this band-limited process, $A(t)$, is described by $N = bT_a$ discrete Fourier coefficients, h_n (say). (Here, both $A(t)$ and h_n are complex.) Let the passband be shifted to the frequency interval $-b/2$ to $+b/2$, and the result transformed back to N complex samples, A_n. (This describes an equivalent complex homodyning, filtering, and discrete sampling process.) As described, the sample interval would be $T_i = b^{-1}$, so that $T_a = NT_i$. To preserve N intervals, let a "zero-th" sample be included, so that the estimate is formed from $(N + 1)$ samples of the band-limited process. In addition, let M be the number of sample intervals per transmitted "pulse length," so $T_p = MT_i$. (Note M need not equal N, but it is assumed that $N \leq M$; i.e., the averaging interval is not greater than the pulse length.)

For T_p smaller than the natural decorrelation time of the scatterers, the $(N + 1)$-square autocovariance matrix can be approximated by

$$K_{mn} \equiv \langle A_m A_n \rangle \approx \left(1 - \frac{|m-n|}{M}\right) e^{j\sigma T_i (m-n)}, \quad \text{(A1)}$$

where $j \equiv -1^{1/2}$, σ is the Doppler shift of the signal, and m, $n = 1$ to $N+1$. This covariance arises from the overlap between the volumes ensonified in the sample h_m versus h_n. Also, for $T_i = b^{-1}$, the white noise component of the received process is independent from one sample to another, so the "noise autocovariance" is just $N_{mn} = \epsilon I_{mn}$, where I_{mn} is the identity matrix and ϵ is the noise variance over signal variance. (Here, both K_{mn} and N_{mn} are normalized by the signal variance, so the total received variance is $1 + \epsilon$. Also, the admitted noise is considered to be essentially "white" across the passband.)

As reported by Theriault (1986), a Cramer-Rao bound on the estimate $\hat{\sigma}$ of the Doppler shift σ is provided by

$$\text{var}(\hat{\sigma} - \sigma) \equiv (\Delta\sigma)^2 \geqslant 1/J(\sigma), \quad \text{(A2)}$$

where $J(\sigma)$ is the "Fisher information matrix." In the present context, $J(\sigma)$ is given by

$$J(\sigma) \equiv \text{Re}\left\{\frac{1}{\epsilon} \text{Trace}\left[\frac{\partial K}{\partial \sigma} * \frac{\partial H}{\partial \sigma}\right]\right\}, \quad \text{(A3)}$$

where the $N+1$ square matrix H is the "optimal filter" for the $N+1$ samples, $\times$ denotes matrix multiplication, and the $\partial/\partial\sigma$ operation is first performed on each element of K and H. The optimal filter H is determined from

$$(K_{km} + \epsilon I_{km}) H_{mn} = K_{kn}. \quad \text{(A4)}$$

If K has an inverse, and for small ϵ (large signal-to-noise ratio), H takes the form

$$H_{mn} = I_{mn} - \epsilon K^{-1}_{mn} + O(\epsilon^2). \quad \text{(A5)}$$

Since I_{mn} is independent of σ, evaluation of A3 centers on K and K^{-1}. For K as given by (A1), the inverse K^{-1} is Hermitian and nearly tri-diagonal, with the first two rows given by

$$K^{-1} \equiv \frac{1}{2} M \times \begin{bmatrix} (1+b) & -e^{j\sigma T_i} & 0 & \cdots & be^{j\sigma T_i N} \\ -e^{-j\sigma T_i} & 2 & -e^{j\sigma T_i} & 0 & \cdots \\ \cdots & & & & \end{bmatrix}, \quad \text{(A6)}$$

where

$$b \equiv 1/(2M - N). \quad \text{(A7)}$$

The last row of K^{-1} is the conjugate-transpose of the first, and the intervening rows are tridiagonal with the same nontrivial elements as the second row. Then

$$\left(\frac{\partial K}{\partial \sigma}\right)_{mn} = jT_i(m-n)\left(1 - \frac{|m-n|}{m}\right) e^{j\sigma T_i (m-n)} \quad \text{(A8)}$$

and

$$\left(\frac{\partial H}{\partial \sigma}\right) = -\epsilon\left(\frac{\partial K^{-1}}{\partial \sigma}\right) = -\frac{1}{2}\epsilon M \begin{bmatrix} 0 & (jT_i)e^{j\sigma T_i} & 0 & \cdots & (jT_i N b)e^{j\sigma T_i N} \\ (jT_i)e^{-j\sigma T_i} & 0 & -(jT_i)e^{j\sigma T_i} & 0 & \cdots \\ \cdots & & & & \end{bmatrix}. \quad \text{(A9)}$$

The first and last diagonal elements of $\partial K/\partial\sigma \times \partial H/\partial\sigma$ thus take the value

$$\left(\frac{\partial K}{\partial \sigma} \times \frac{\partial H}{\partial \sigma}\right)_{nm} = \frac{1}{2}\epsilon T_i^2 (M - 1 - bN^2(M-N)), \quad n = 1 \text{ or } N+1, \quad \text{(A10)}$$

and the intermediate diagonals are

$$\left(\frac{\partial K}{\partial \sigma} \times \frac{\partial H}{\partial \sigma}\right)_{nm} = \epsilon T_i^2 (M-1), \quad n = 2 \text{ to } N. \quad \text{(A11)}$$

There are 2 of (A10) and $(N-1)$ of (A11), so that J has the value

$$J(\sigma) = NT_i^2\left[M - 1 - N\left(\frac{M-N}{2M-N}\right)\right] = T_a\left[T_p - T_i - T_a\left(\frac{T_p - T_a}{2T_p - T_a}\right)\right] \quad \text{(A12)}$$

(see Fig. 11). The Doppler estimate variance $(\Delta\sigma)^2$ is just the reciprocal of this, which (notably) is independent of ϵ as $\epsilon \to 0$. For $T_i \ll T_p$ and $T_a = T_p$, this reduces to Theriault's (1986) result; i.e.,

$$(\Delta\sigma)^2 \equiv J^{-1} \to T_p^{-2}. \quad \text{(A13)}$$

As noted by Theriault (1986), (A12) and (A13) should provide reasonable but somewhat optimistic lower bounds on the uncertainty of the Doppler estimates, in this case for a band-pass filtered signal where independent samples lie at intervals T_i apart. Note that, even if the process is oversampled (i.e., $T_i < b^{-1}$), the total information content must still have the same bound. Thus, T_i can be replaced by b^{-1} (the inverse bandwidth of the system) in (A12), as long as the sample rate is sufficient; i.e., $T_i \leqslant b^{-1}$. If $T_i > b^{-1}$, on the other hand, information is lost and T_i is the appropriate choice. Worse, the results may be further degraded by aliasing in this case.

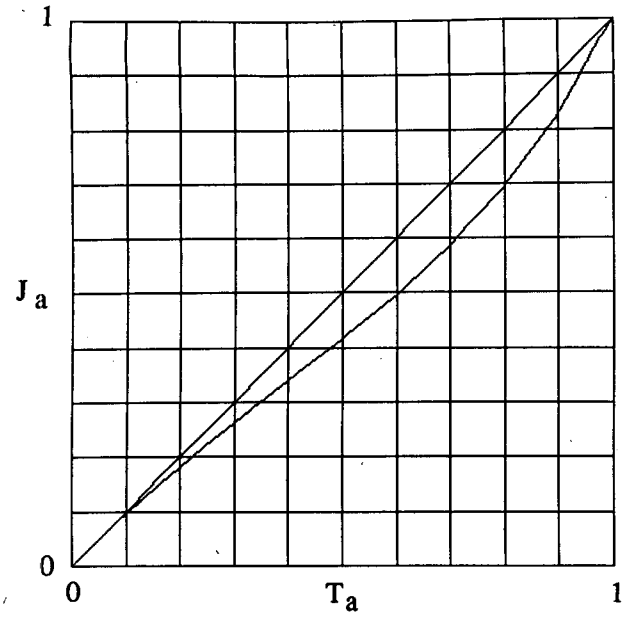

FIG. 11. The "Fisher information content" J_a (the inverse of the Doppler estimate variance) vs averaging time T_a, with a fixed pulse length, T_p. The curving line is J_a vs T_a; the straight line shows $J_a = T_a$ for reference. Here, J_a is normalized by the value at $T_a = T_p$, and T_a is normalized by T_p. The slope of J_a vs T_a equals that of the straight line at the two ends ($T = 0$ and $T = 1$), but the curve drops below the straight line for intermediate values of T_a. This indicates that as T_a is decreased below 1, information is lost more quickly than in a corresponding white noise process. The form of this curve suggests that it is appropriate to set $T_a \equiv T_p$. (Of course, this conclusion may not apply for the suboptimal covariance technique actually employed.)

It is worth reiterating that this result is independent of the signal to noise ratio (as long as it is large). This Doppler estimation error is often interpreted as "self clutter," due to finite returns from the nonoverlapping regions of the volumes ensonified at different times.

APPENDIX B

Bubble Scattering Near the Surface

The resonant frequency of a given bubble is very nearly proportional to $P^{1/2}/a$, where P is the pressure and a the bubble's radius (Urick 1975; Clay and Medwin 1977). At 1 atmosphere pressure and 15°C, the resonant frequency in Hz is roughly $f_r \approx 3.26 \text{ m s}^{-1}/a$ (Urick 1975). The scattering cross section σ_s of a bubble is described by

$$\sigma_s \approx \frac{4\pi a^2}{((f_r/f)^2 - 1)^2 + \delta^2}, \qquad \text{(B1)}$$

where f is the incident sonar frequency, and δ is the damping coefficient of the resonance ($\delta \approx \Delta f$, where Δf is the "bandwidth" between the half-power points of the forced oscillation; e.g., see Clay and Medwin 1977). The net backscattering strength per unit volume is then

$$s_v(z) \approx \frac{1}{4\pi} \int_{a=0}^{\infty} \sigma_s(a, z) p(a, z) da, \qquad \text{(B2)}$$

where p is the probability density of bubbles per unit volume per radius-increment da. For bubbles with radius $a \approx 50$ to 200 μm or so, $p(a) \approx a^{-4}$ (Crawford and Farmer 1987; Johnson and Cooke 1979; Medwin 1970, 1977). Measurements made optically show a decrease in $p(a)$ for $a < 50$ μm ($f_r \approx 65$ kHz) which may (or may not) be due to photographic resolution (Johnson and Cooke 1979; Walsh and Mulhern 1987). Acoustic measurements, on the other hand, indicate that the a^{-4} dependence extends down past 40 μm ($f_r \approx 80$ kHz), perhaps even past 20 μm ($f_r \approx 160$ kHz) in radius (Medwin 1970, 1977). The a^{-4} dependence cannot extend indefinitely in either direction: since the volume of a bubble is proportional to a^3, the total volume fraction of air depends logarithmically on both the upper and lower cutoffs of the a^{-4} region. For $p(a) \approx a^{-4}$, and for δ^2 small, the integral (B2) yields s_v directly proportional to f. For frequencies higher than the cutoff of the bubble spectrum, s_v becomes roughly constant, proportional to the total surface area of all the bubbles.

The surface-backscatter coefficient s_s is four times the vertical-integral of s_v (neglecting beam-pattern variations and absorption across the thickness of the bubble layer, and including the mirror images due to reflections off the surface). The data shown in Fig. 4 (from Urick 1975) indicates $S_s \approx -40$ dB at 60 kHz and with 5 m s^{-1} (10 knots) of wind. Alternatively, a vertical integral of the bubble densities and cross sections described by Crawford and Farmer (1987) for 119 kHz sound yields $S_s \approx -42$ dB at a nominal 5 m s^{-1} windspeed. Since both estimates have at least a ±5 dB uncertainty, these are consistent with either frequency-dependence described above ($s_s \propto f$ or constant). If the backscatter doesn't vary with frequency over 60 kHz, a compromise value of $S_s = -40$ dB at 5 m s^{-1} is suggested, yielding

$$S_s \approx -40 \text{ dB} + 30 \log(W_*), \qquad \text{(B3)}$$

where $W_* \equiv W/(5 \text{ m s}^{-1})$.

APPENDIX C

Saturation

For spherically spreading sound, expressions for r_L and r_s are as follows (Shooter et al. 1974):

$$r_s = r_1 e^{1/\beta\epsilon k r_1} \qquad \text{(C1)}$$

$$(a r_L)^{-1} = (\beta\epsilon k r_1) + \ln(r_L/r_1), \qquad \text{(C2)}$$

where r_1 is the radius of the (equivalent) spherical source, β is a constant depending on the equation of state of the water (with a value of 3.5 for water at 20°C, or 3.3 at 10°C; e.g., see Clay and Medwin 1977), $k = 2\pi f/c$ is the wavenumber of the sound, $a = \frac{1}{2}A$

$= \alpha/(20 \log e)$ is the attenuation rate for the pressure amplitude, and $\epsilon = P_1/\rho c^2$ is a measure of the acoustic steepness at the source, where $P(r_1) = P_1 \sin\omega t$ (for example). Setting $r_L = r_s$ then leads to a "critical source level" ϵ_c, for which shocks just barely (don't) form as linear behavior is restored:

$$\beta k \epsilon_c r_1 = 2ar_L = Ar_L, \tag{C3}$$

where r_L (and hence r_s also) is the solution of

$$(Ar_L) \ln(r_L/r_1) = 1. \tag{C4}$$

(Here, $\ln x$ is the natural logarithm.) Two more items require discussion: 1) the "source radius" r_1, and 2) conversion of the "source pressure" $P_1 = \epsilon\rho c^2$ to the equivalent intensity (or pressure) at a nominal distance of 1 meter from the origin of the spherical spreading. For piston sources, Shooter et al. (1974) suggest a value for r_1 between $R/3$ and $3R/4$, where the "Rayleigh distance" R is the transducer area divided by the wavelength of the transmitted sound. Since r_L as a solution of (C4) is approximately logarithmically dependent on r_1, this uncertainty has minimal effect on the results. The log-average value is just $R/2$. For spherically spreading waves, the linear evolution equation for pressure is

$$P(r) = P_S r^{-1} e^{-a(r-1)}, \tag{C5}$$

where P_S is the rms pressure at 1 meter from the origin of spreading. Now P_1 from above is the peak pressure amplitude, so the rms pressure at r_1 is just $2^{-1/2}P_1$, yielding

$$P_S = 2^{-1/2} P_1 r_1 e^{\alpha(r_1-1)} \approx 2^{-1/2} \rho c^2 A r_L / \beta k r_0, \tag{C6}$$

where $r_0 \equiv 1$ m. For example, in seawater at 15°C, 35 ppt, and for 200 kHz sound with $r_1 = 1$ meter, P_S is about 1.8 atm (i.e., using $\rho = 1026$ kg m^{-3}, $c = 1500$ m s^{-1}, $A = 0.12$ m^{-1}, $\beta = 3.4$, and $k = 2\pi f/c = 838$ m^{-1}). For a 1 cm by 50 cm bar, $R/3 \approx 0.22$ cm, and P_S would be reduced to 1.3 atm (each example requires solving C4).

APPENDIX D

The Admitted Noise Bandwidth

Start with the complex, discrete time series A_n as in Eq. (1) and appendix A. For simplicity, let $T_a = T_p \equiv T$, so the signal autocovariance drops to zero at an interval equal to the averaging time. Covariance estimates at the lag $T_i = T/M$ are formed as in Eq. (1). Then $\hat{C}_1$ has the expected value of the actual signal + noise covariance at this lag: $\langle \hat{C}_1 \rangle = C_1{}^S + C_1{}^N$. For the lag value $1/b$, of course, $\langle C_1{}^N \rangle \equiv 0$. Statistical sampling error, however, causes fluctuations about $C_1{}^S$. To evaluate this effect, examine

$$\begin{aligned}
\langle |\hat{C}_1|^2 \rangle &\equiv \frac{1}{M^2} \sum_i^M \sum_j^M \langle A_i A_{i-1}^* A_j^* A_{j-1} \rangle \\
&\approx \frac{1}{M^2} \sum_i^M \sum_j^M \{ \langle A_i A_{i-1}^* \rangle \langle A_j^* A_{j-1} \rangle \\
&\quad + \langle A_i A_j^* \rangle \langle A_{i-1}^* A_{j-1} \rangle + \langle A_i A_{j-1} \rangle \langle A_{i-1}^* A_j^* \rangle \} \\
&\approx |C_1|^2 + \frac{1}{M} |C_0|^2 + 2 \frac{M-1}{M^2} |C_1|^2 \\
&\quad + 2 \frac{M-2}{M^2} |C_2|^2 + \cdots + \frac{2}{M^2} |C_{M-1}|^2, \qquad \text{(D1)}
\end{aligned}$$

where C_m is the covariance at lag m, $C(mT/M)$, and the samples A_n are assumed to be normally distributed. For pulse length T, the signal covariance is approximately a linear ramp dropping to zero at lag T [i.e., as in (A1)]. Letting $|C_m{}^S| \approx C_0{}^S(1 - m/M)$, the "signal part" of the terms after the first one in (D1) approach the integral of $2x^3$ from 0 to 1 times $|C_0{}^S|^2$ for large M, giving $\frac{1}{2}|C_0{}^S|^2$ as an approximate total. For $M = bT$, the expected lag-1 noise covariance $C_1{}^N$ would be zero; however, for a slightly smaller sample interval (so that $C_1{}^N \neq 0$ but $C_m{}^N \to 0$ for $m > 1$), we can write

$$\begin{aligned}
\langle |\hat{C}_1|^2 \rangle &\approx |C_1|^2 + \frac{1}{2} |C_0{}^S|^2 \\
&\quad + (bT)^{-1} |C_0{}^N|^2 + |C_1{}^N|^2. \qquad \text{(D2)}
\end{aligned}$$

Note that, even if $M > bT$ (i.e., with oversampling), there are only bT degrees of freedom working to reduce the sample error [the third term in (D2)]. The last term, $|C_1{}^N|^2$, arises from a bias toward the center-frequency of the pass-band. This bias can be removed using a reasonable model of the noise and filtering, leaving just the true lag-one covariance squared plus the sample error variance. The total noise variance admitted through the band-pass filter is $C_0{}^N = bH$, where H is the noise spectral level as in (62). The net sample error is therefore just $(b/T)H^2$. This corresponds to an effective noise bandwidth of $(b/T)^{1/2}$.

REFERENCES

Clay, C. S., and H. Medwin, 1977: *Acoustical Oceanography: Principles and Applications.* Wiley Interscience Press, 544 pp.

Crawford, G. B., and D. M. Farmer, 1987: On the spatial distribution of ocean bubbles. *J. Geophys. Res.*, **92**, 8231–8243.

Donelan, M. A., J. Hamilton and W. H. Hui, 1985: Directional spectra of wind generated waves. *Phil. Trans. Roy. Soc. London,* 315, 509–562.

Fisher, F. H., and V. P. Simmons, 1977: Sound absorption in water. *J. Acoust. Soc. Amer.*, **62**, 558–564.

Johnson, B. D., and R. Cooke, 1979: Bubble populations and spectra in coastal waters. *J. Geophys. Res.*, **84**, 3761–3766.

Long, S. R., and N. E. Huang, 1976: On the variation and growth of waveslope spectra in the capillary-gravity range with increasing wind. *J. Fluid Mech.*, **77**, 209–228.

Longuet-Higgins, M. S., 1948: Sea waves and microseisms. *Nature,* **162,** 700.

McDaniel, S. T., and A. D. Gorman, 1982: Acoustic and radar sea surface backscatter. *J. Geophys. Res.,* **87,** 4127–4136.

Medwin, H., 1970: In-situ acoustic measurements of bubble populations in coastal ocean waters. *J. Geophys. Res.,* **75,** 599–611.

——, 1977: In-situ acoustic measurements of microbubbles at sea. *J. Geophys. Res.,* **82,** 971–976.

Miller, K. S., and M. M. Rochwarger, 1972: A covariance approach to spectral moment estimations. *I.E.E.E. Trans. Inf. Theory,* **5,** 588–596.

Phillips, O. M., 1977: *The Dynamics of the Upper Ocean.* Cambridge University Press, 336 pp.

——, 1985: Spectral and statistical properties of the equilibrium range in wind generated gravity-waves. *J. Fluid Mech.,* **156,** 505–531.

Pinkel, R., 1981: On the use of Doppler sonar for internal wave measurements. *Deep Sea Res.,* **28A,** 269–289.

——, and J. A. Smith, 1987: Open ocean surface wave measurement using Doppler sonar. *J. Geophys. Res.,* **92,** 12 967–12 973.

Rummler, W. D., 1968: Introduction of a new estimator for velocity spectral parameters. Bell Telephone Lab. Rep. MM-68-4141-5, Murray Hill, N.J.

Shooter, J. A., T. G. Muir and D. T. Blackstock, 1974: Acoustic saturation of spherical waves in water. *J. Acoust. Soc. Amer.,* **55,** 54–62.

Smith, J. A., R. Pinkel and R. A. Weller, 1987: Velocity structure in the mixed layer during MILDEX. *J. Phys. Oceanogr.,* **17,** 425–439.

Theriault, K. B., 1986: Incoherent multibeam Doppler current profiler performance. Part I: Estimate variance. *I.E.E.E. J. Ocean Eng.,* **0E-11**(1), 7–15.

Thorpe, S. A., 1986: Bubble clouds: a review of their detection by sonar, of related models, and of how K_v may be determined. *Oceanic Whitecaps,* Reidel Publishing, 57–68.

Urick, R., 1975: *Principles of Underwater Sound.* McGraw-Hill, 384 pp.

Walsh, A. L., and P. J. Mulhearn, 1987: Photographic measurements of bubble populations form breaking wind waves at sea. *J. Geophys. Res.,* **92,** 14 553–14 566.